Soil nitrous oxide emissions across the northern high latitudes

Naiqing Pan[1], Hanqin Tian[1,2*], Hao Shi[3], Shufen Pan[4,1], Josep G. Canadell[5], Jinfeng Chang[6], Philippe Ciais[7], Eric A. Davidson[8], Gustaf Hugelius[9,10], Akihiko Ito[11], Robert B. Jackson[12], Fortunat Joos[13], Sebastian Lienert[13], Dylan B. Millet[14], Stefan Olin[15], Prabir K. Patra[16], Rona L. Thompson[17], Nicolas Vuichard[7], Kelley C. Wells[14], Chris Wilson[18,19], Yongfa You[1], Sönke Zaehle[20]

[1]Center for Earth System Science and Global Sustainability, Schiller Institute for Integrated Science and Society, Boston College, Chestnut Hill, MA, USA

[2]Department of Earth and Environmental Sciences, Boston College, Chestnut Hill, MA, USA

[3]State Key Laboratory of Urban and Regional Ecology, Research Center for Eco-Environmental Sciences, Chinese Academy of Sciences, Beijing, China

[4]Department of Engineering and Environmental Studies Program, Boston College, Chestnut Hill, MA, USA

5Global Carbon Project, CSIRO Oceans and Atmosphere, Canberra, Australian Capital Territory, Australia

[6] College of Environmental and Resource Sciences, Zhejiang University, Hangzhou, China

[7]Laboratoire des Sciences du Climat et de l'Environnement, LSCE, CEA CNRS, UVSQ UPSACLAY, Gif sur Yvette, France

[8]Appalachian Laboratory, University of Maryland Center for Environmental Science, Frostburg, MD, USA

[9]Department of Physical Geography, Stockholm University, Stockholm, Sweden

[10] Bolin Centre for Climate Research, Stockholm University, Stockholm, Sweden

[11] National Institute for Environmental Studies, Tsukuba, Japan

[12] Department of Earth System Science, Woods Institute for the Environment, Precourt Institute for Energy, Stanford University, Stanford, CA, USA

[13] Climate and Environmental Physics, Physics Institute and Oeschger Centre for Climate Change Research, University of Bern, Bern, Switzerland

[14] Department of Soil, Water, and Climate, University of Minnesota, St Paul, MN, USA

[15] Department of Physical Geography and Ecosystem Science, Lund University, Lund, Sweden

[16] Research Institute for Global Change, JAMSTEC, Yokohama, Japan

[17] Norsk Institutt for Luftforskning, NILU, Kjeller, Norway

[18] National Centre for Earth Observation, University of Leeds, Leeds, UK

[19] Institute for Climate and Atmospheric Science, School of Earth & Environment, University of Leeds, Leeds, UK

[20] Max Planck Institute for Biogeochemistry, Jena, Germany

*Corresponding author: Hanqin Tian (hanqin.tian@bc.edu)

Geophysical Research Letters (Submitted on January 18, 2024)

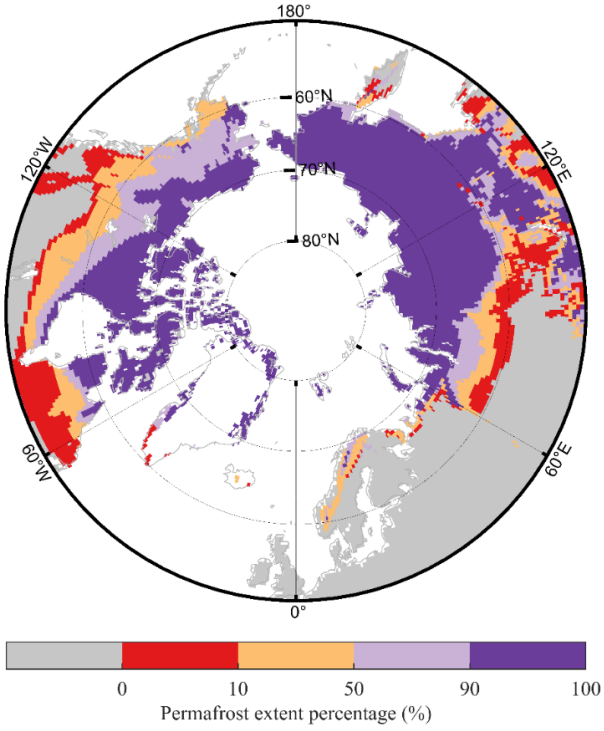

Fig. S1: Spatial distribution of the percentage of permafrost extent in the Northern Hemisphere.

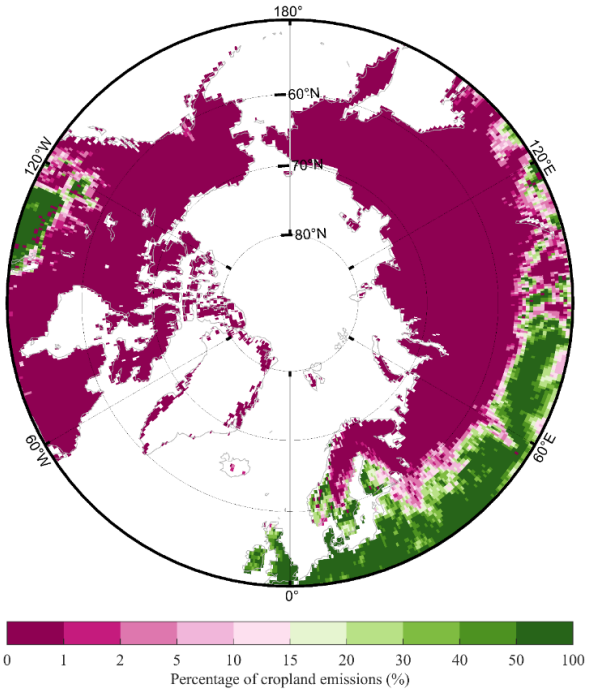

Fig. S2: Spatial distribution of the percentage of soil N_2O emissions from croplands.

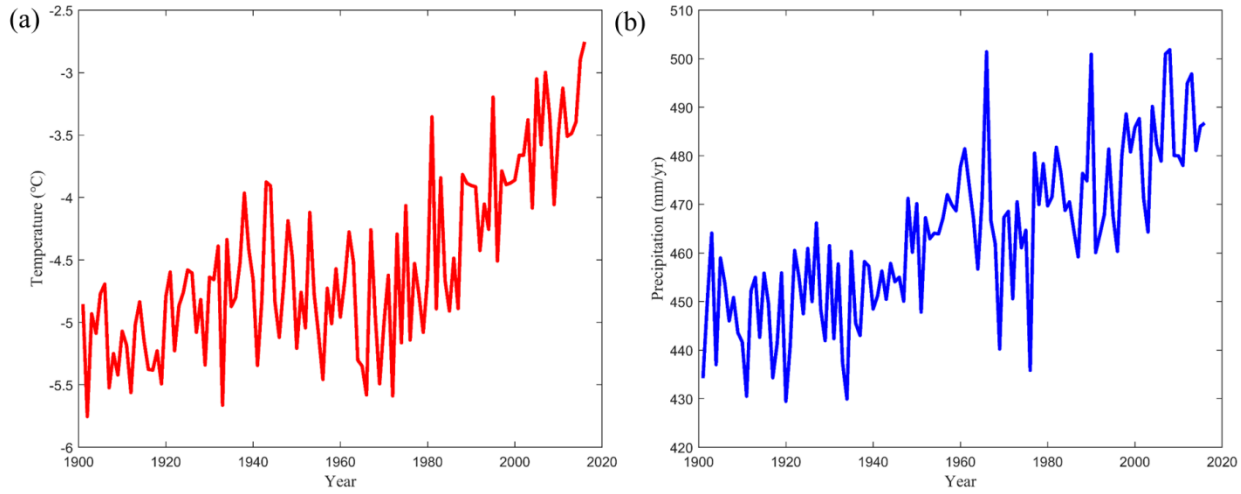

Fig. S3: Temporal variations in mean temperature (a) and precipitation (b) of the northern high latitudes during 1901-2016.

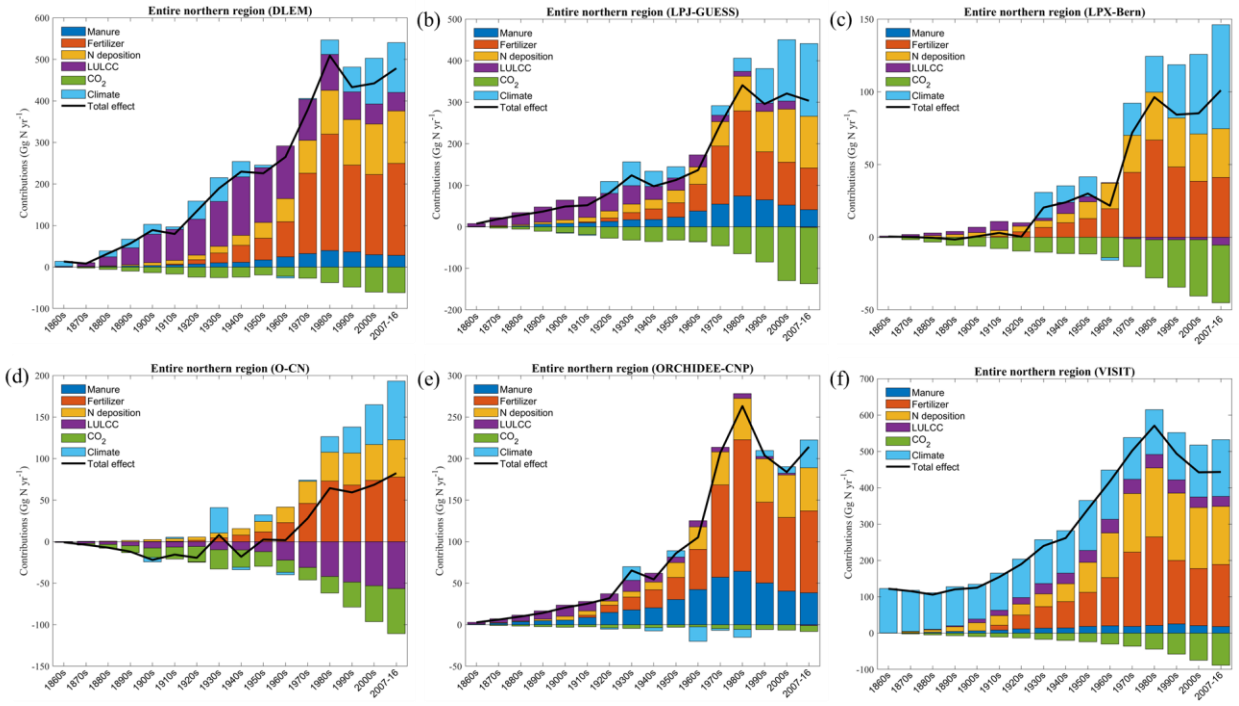

Fig. S4: Decadal variations in the contributions of different driving factors to soil N_2O emissions from the entire northern high latitudes estimated by individual NMIP model.

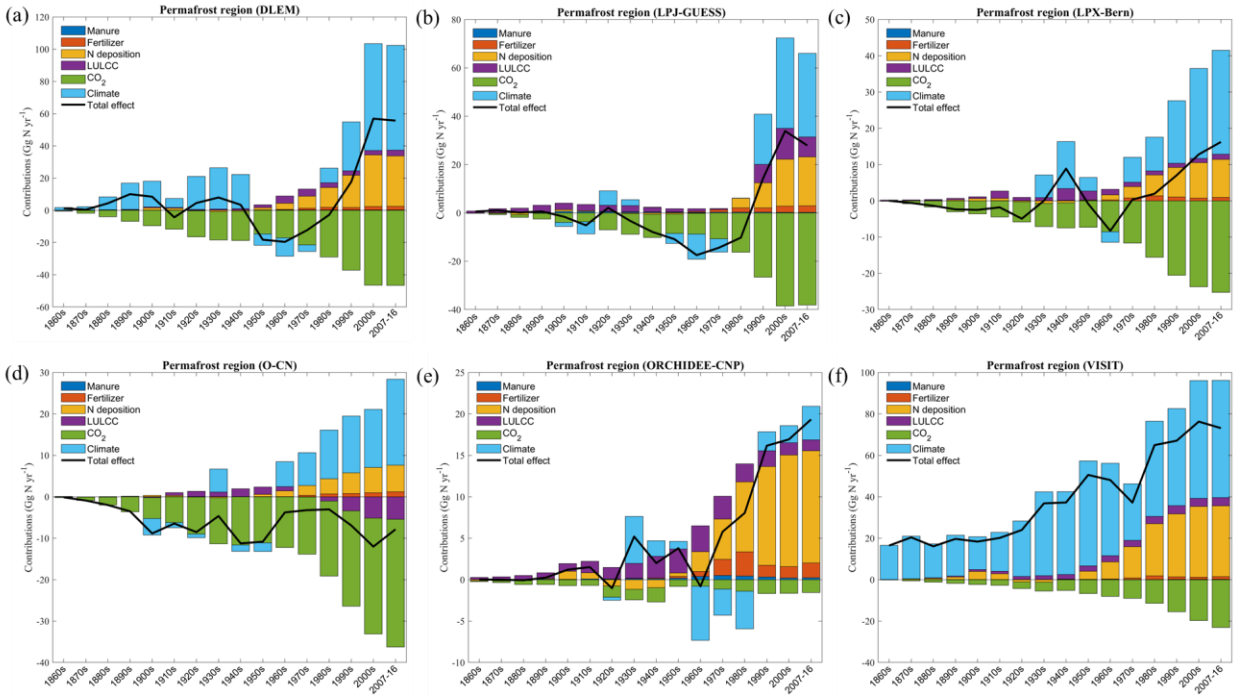

Fig. S5: Decadal variations in the contributions of different driving factors to soil N_2O emissions from permafrost regions estimated by individual NMIP model.

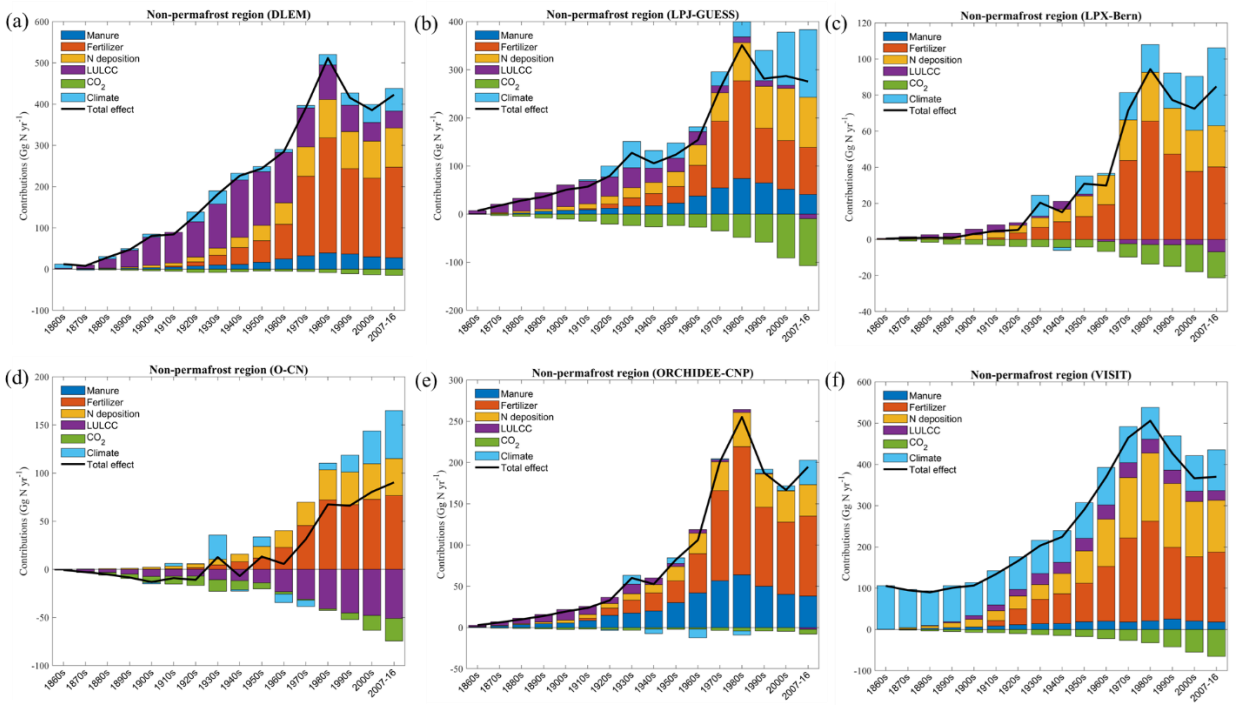

Fig. S6: Decadal variations in the contributions of different driving factors to soil N_2O emissions from non-permafrost regions estimated by individual NMIP model.

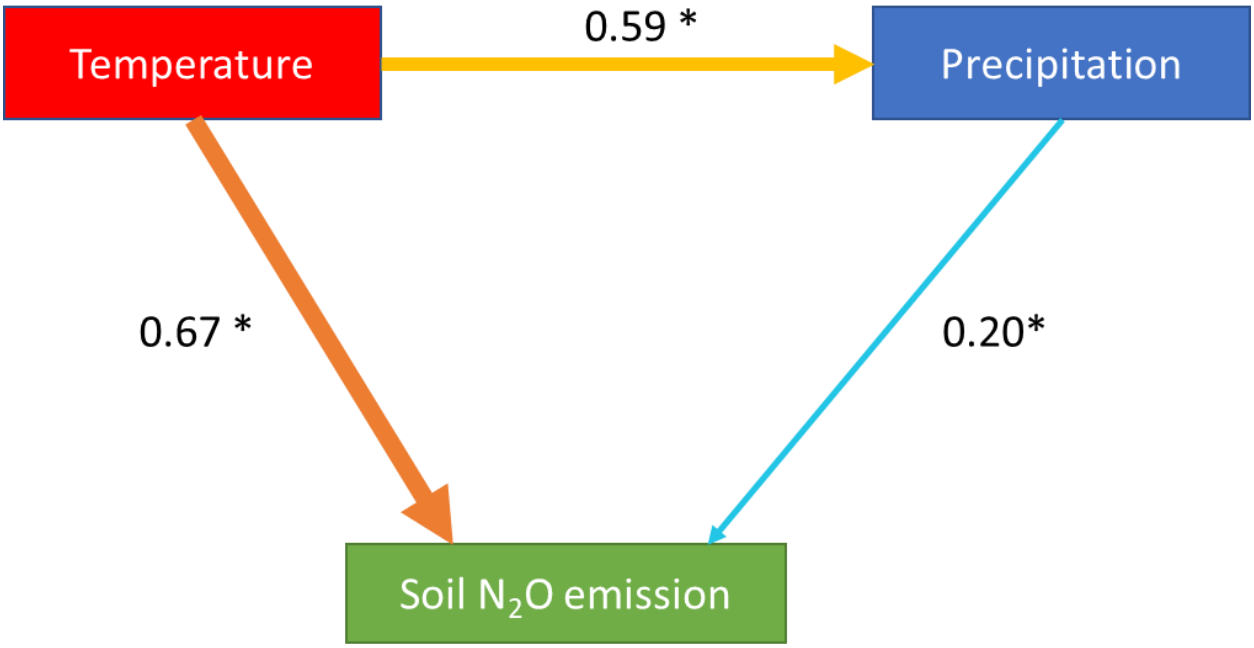

Fig. S7: Path analysis results. Numbers adjacent to arrows in the path diagrams are standardized path coefficients indicating the magnitude of the influence between factors, and the significance level is indicated by * ($p < 0.01$).

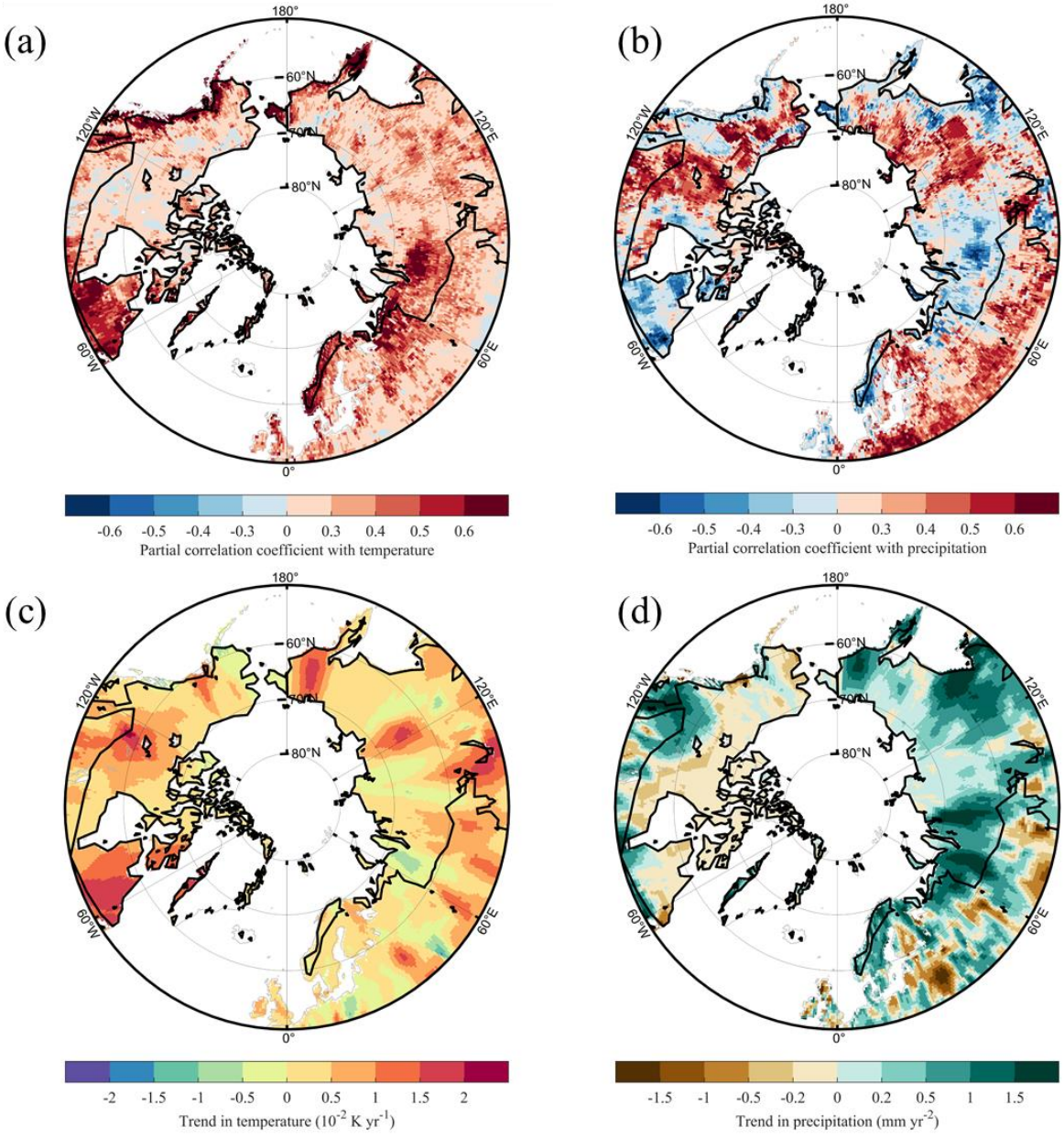

Fig. S8: Spatial distributions of the partial correlation coefficients between modelled annual soil N_2O emissions and temperature (a) and precipitation (b) during 1901-1980; (c) and (d) show trends in temperature and precipitation during 1901-1980, respectively. The black lines in (a)-(d) show the extent of the permafrost region.

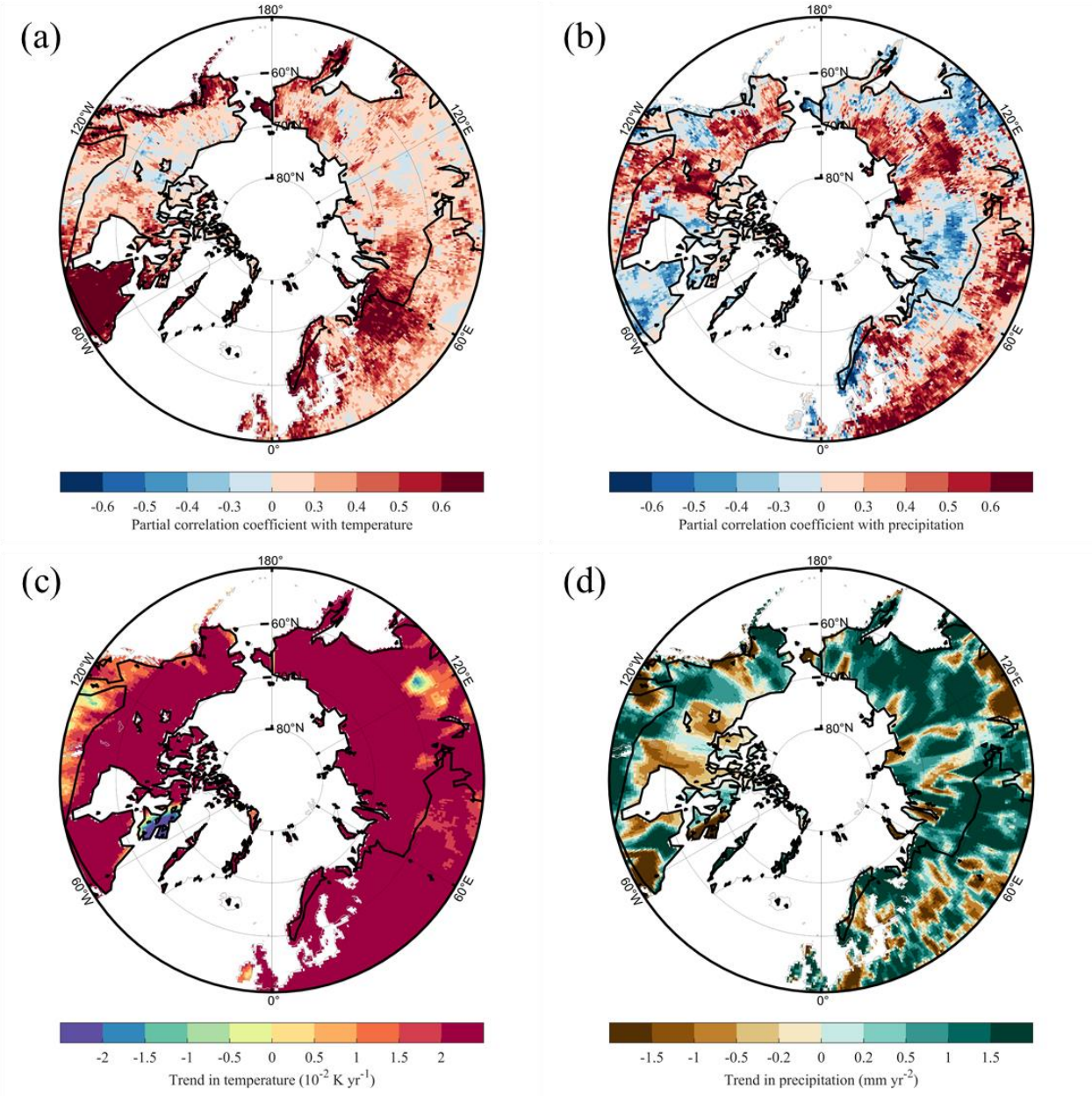

Fig. S9: Spatial distributions of the partial correlation coefficients between modelled annual soil N_2O emissions and temperature (a) and precipitation (b) during 1980-2016; (c) and (d) show trends in temperature and precipitation during 1980-2016, respectively. The black lines in (a)-(d) show the extent of the permafrost region.

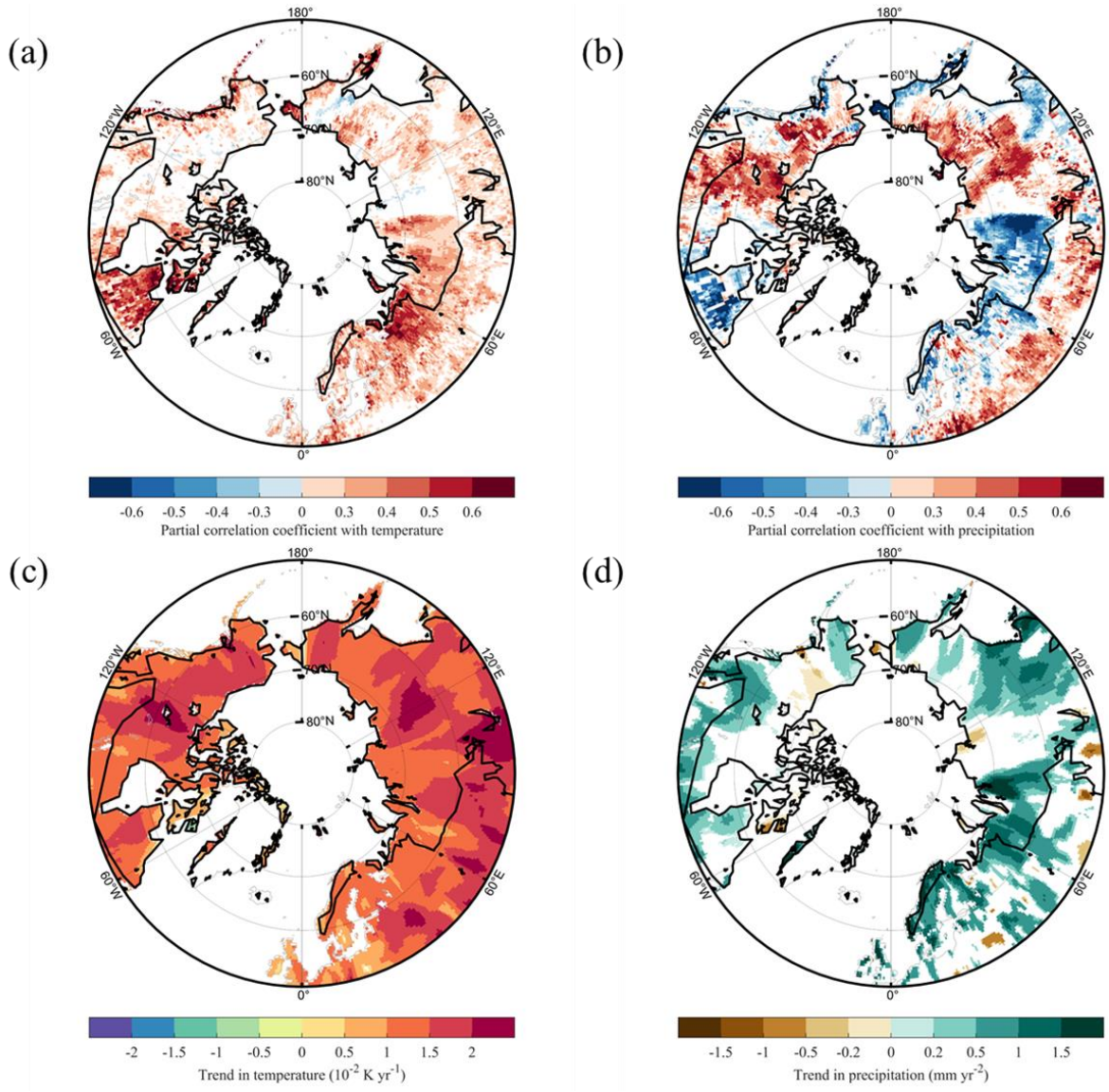

Fig. S10: Trends in temperature and precipitation and their partial correlation coefficients with soil N_2O emissions. a and b show spatial distributions of the partial correlation coefficients for modelled annual soil N_2O emissions versus temperature and precipitation during 1901-2016; grids with non-significant correlation (p>=0.05) were excluded. c and d show trends in temperature and precipitation during 1901-2016, respectively; grids with non-significant trends (*p*>=0.05) were excluded. The black lines in (a)-(d) show the extent of the permafrost region.

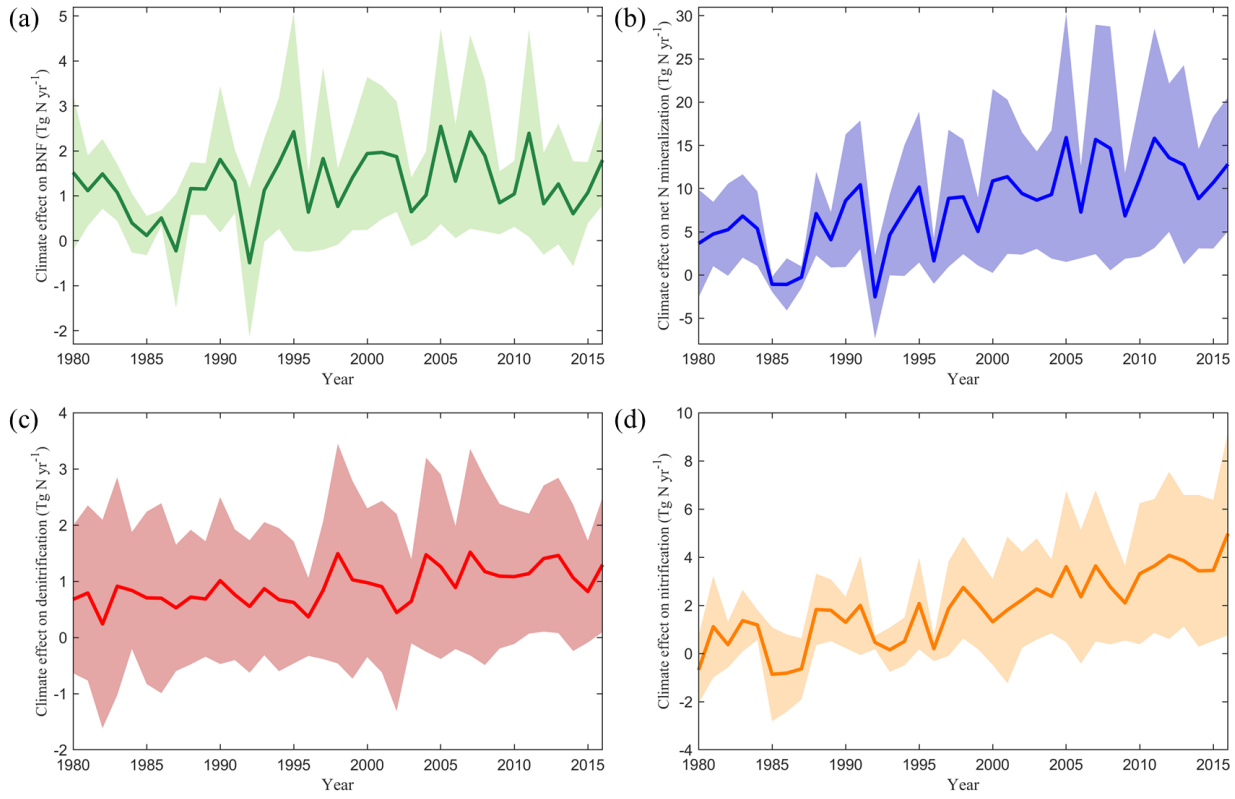

Fig. S11: Climate effects on reactive N flows of the northern high latitudes. (a)-(d) show the effects of climate change on regional biological N fixation, net N mineralization, denitrification, and nitrification, respectively, the lines represent the ensemble means of NMIP model estimates and the shaded areas indicate one standard deviation of model estimates.

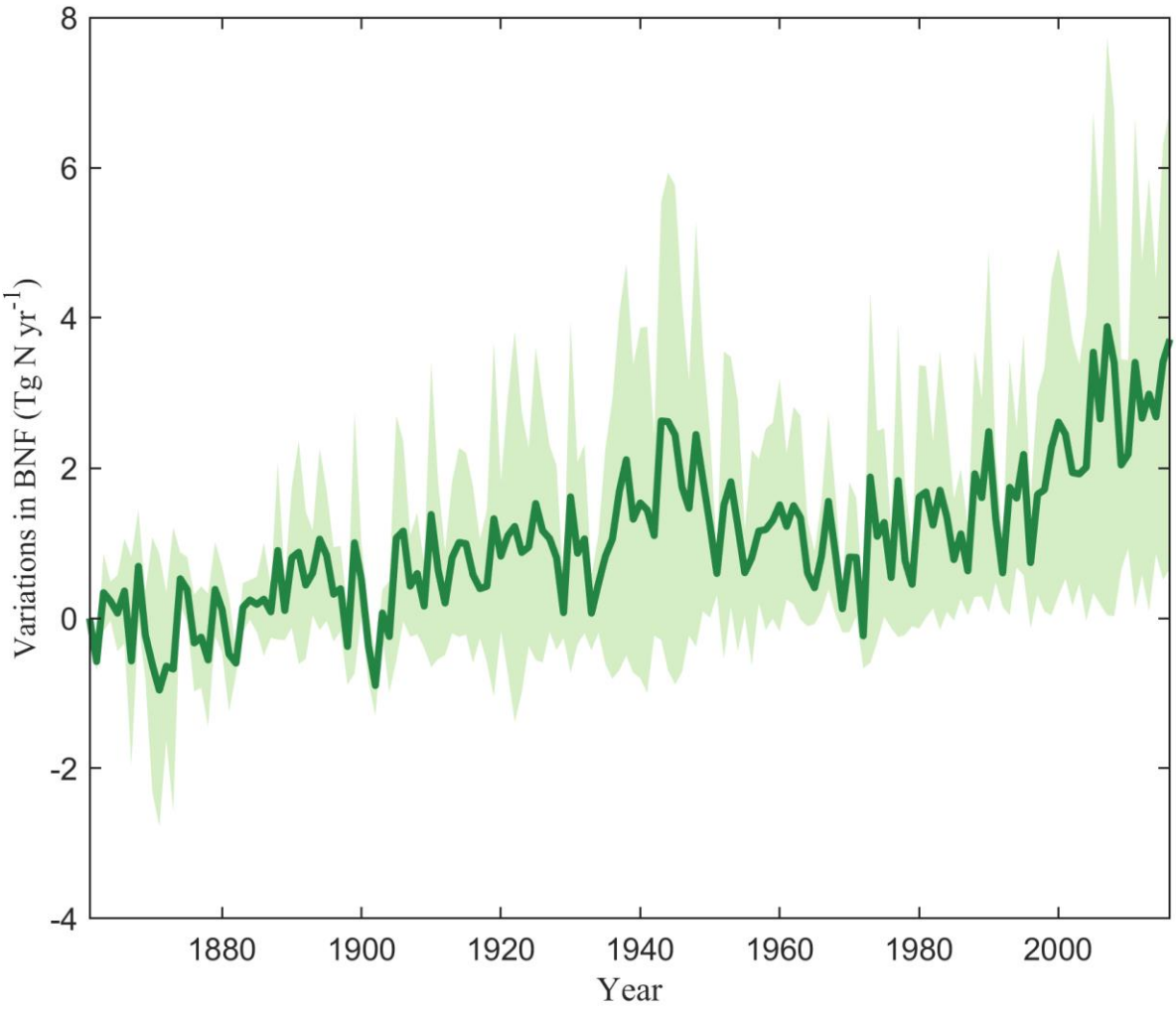

Fig. S12: Temporal variations in the total biological nitrogen fixation in the northern high latitudes during 1861-2016. The line represents the ensemble means of NMIP model estimates and the shaded area indicates one standard deviation of model estimates.

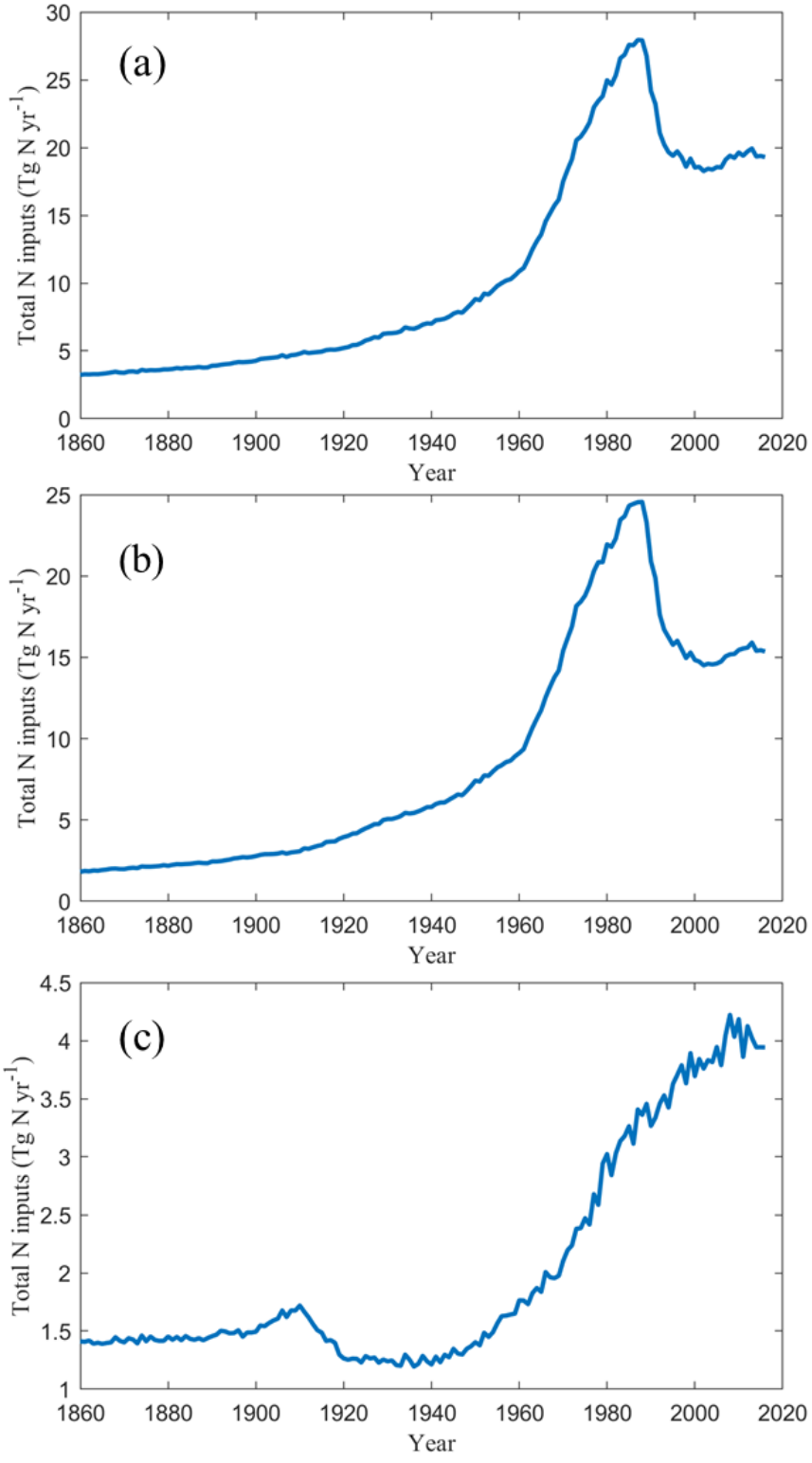

Fig. S13: Temporal variations in the total N inputs in entire northern high latitudes (a), non-permafrost region (b) and permafrost region (c).

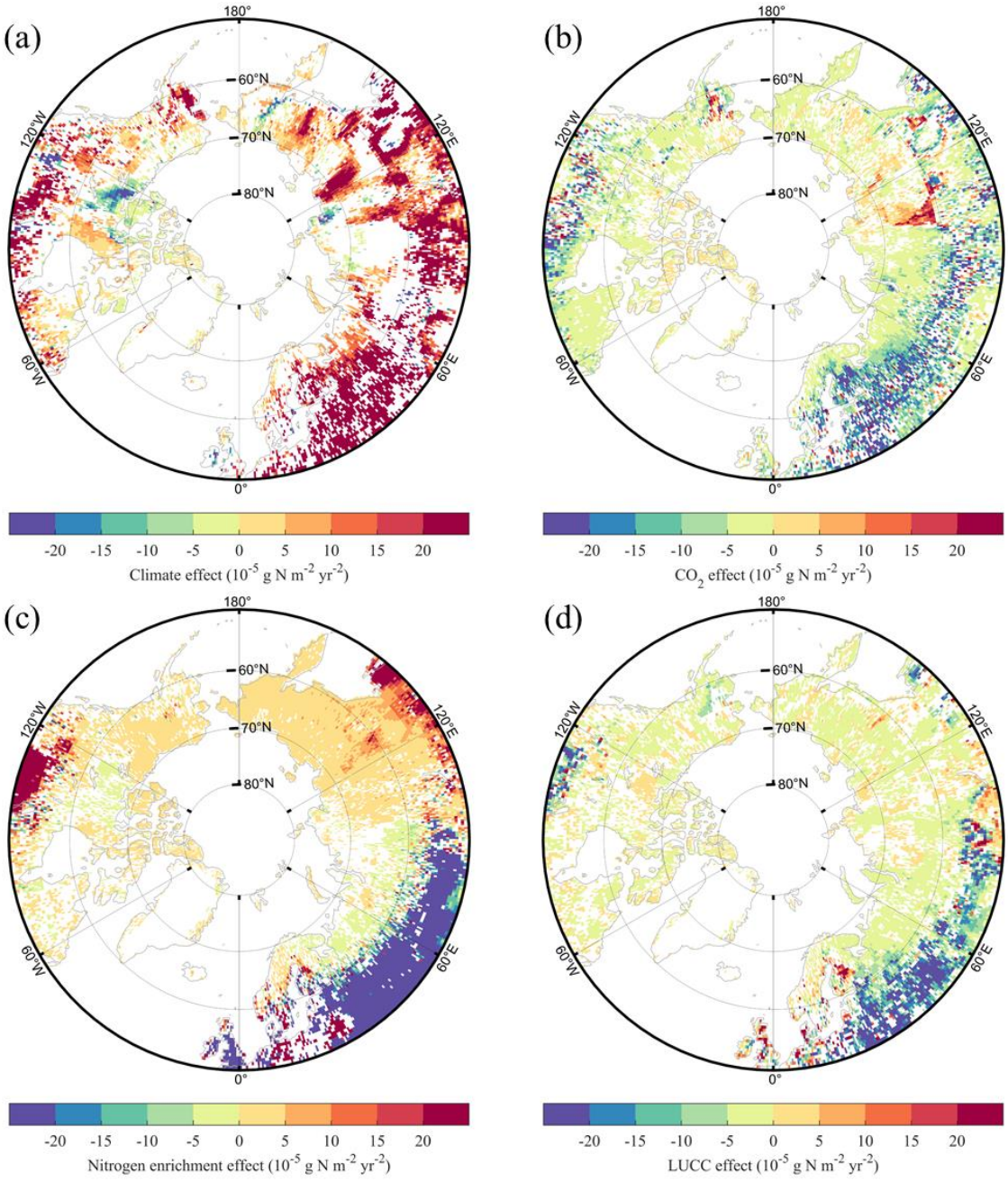

Fig. S14: Spatial patterns of the effects of different driving factors during the period 1980-2016. (a)-(d) show the effects of climate, CO_2, nitrogen enrichment and LULCC, respectively. Grids with non-significant trends (p>=0.05) were excluded.

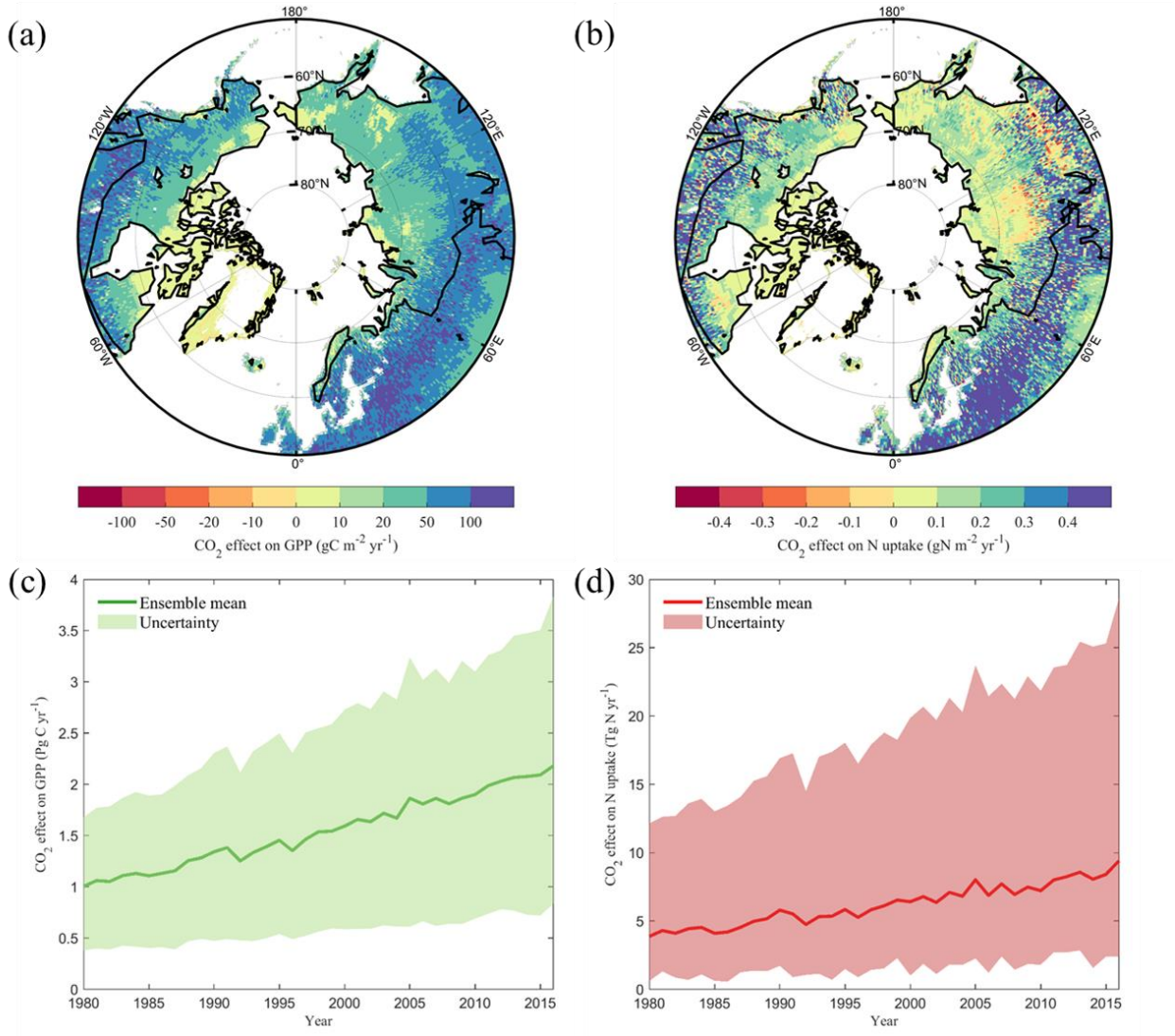

Fig. S15: The effects of increasing CO_2 concentration on ecosystem GPP and plant nitrogen uptake. (a) and (b) show spatial distributions of modelled average CO_2 effects on GPP and nitrogen uptake during 1980-2016, respectively; black lines show the extent of the permafrost region. (c) and (d) show the temporal variations in CO_2 effects on regional GPP and nitrogen uptake, respectively; the lines represent the ensemble means of all NMIP model estimates and the shaded areas show minimum and maximum estimates.

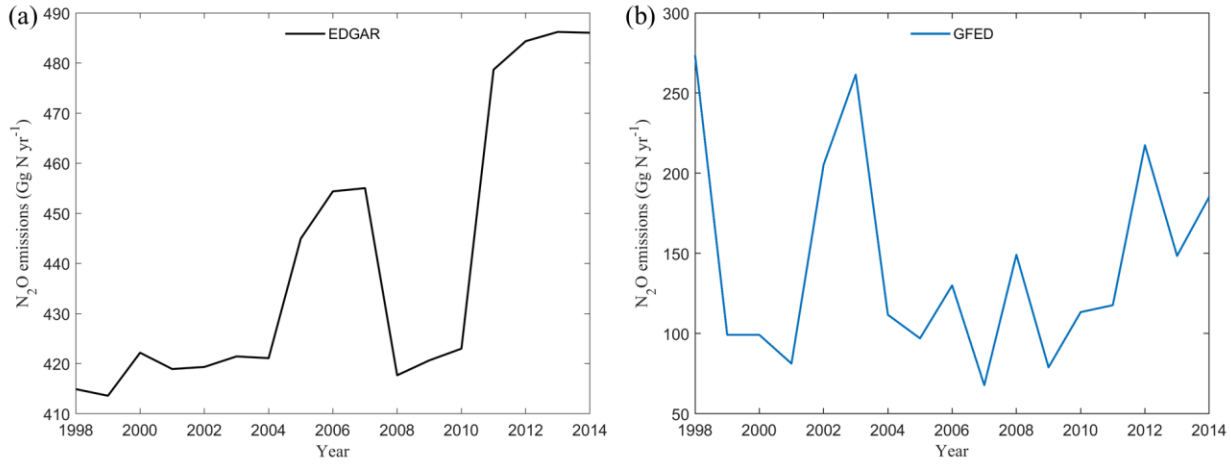

Fig. S16: Interannual variations in N_2O emissions from non-soil anthropogenic sources (a) and biomass burning (b).

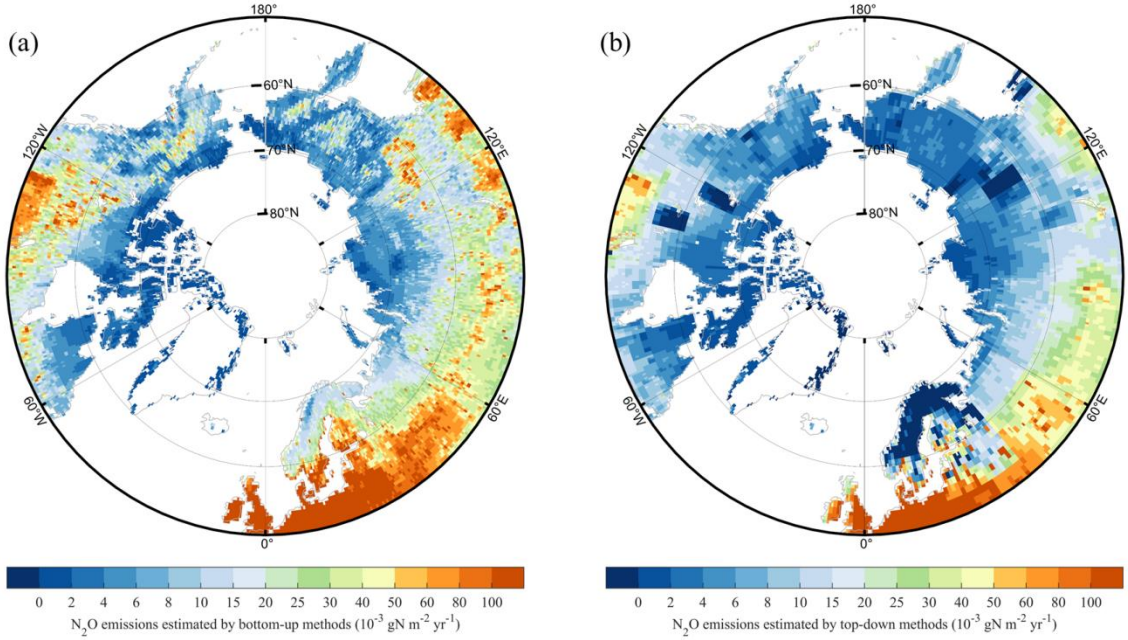

Fig. S17. Uncertainty in soil N_2O emissions estimated by NMIP models (a) and in total N_2O emissions estimated by top-down models (b). Here, one standard deviation of all model estimates was used to indicate uncertainty.

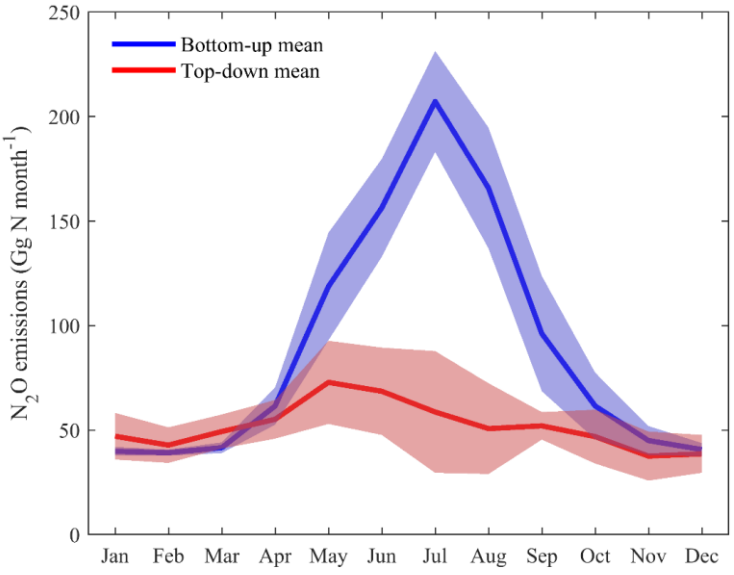

Fig. S18. Comparison of intra-annual fluctuations of N_2O emissions estimated by TD and BU approaches.

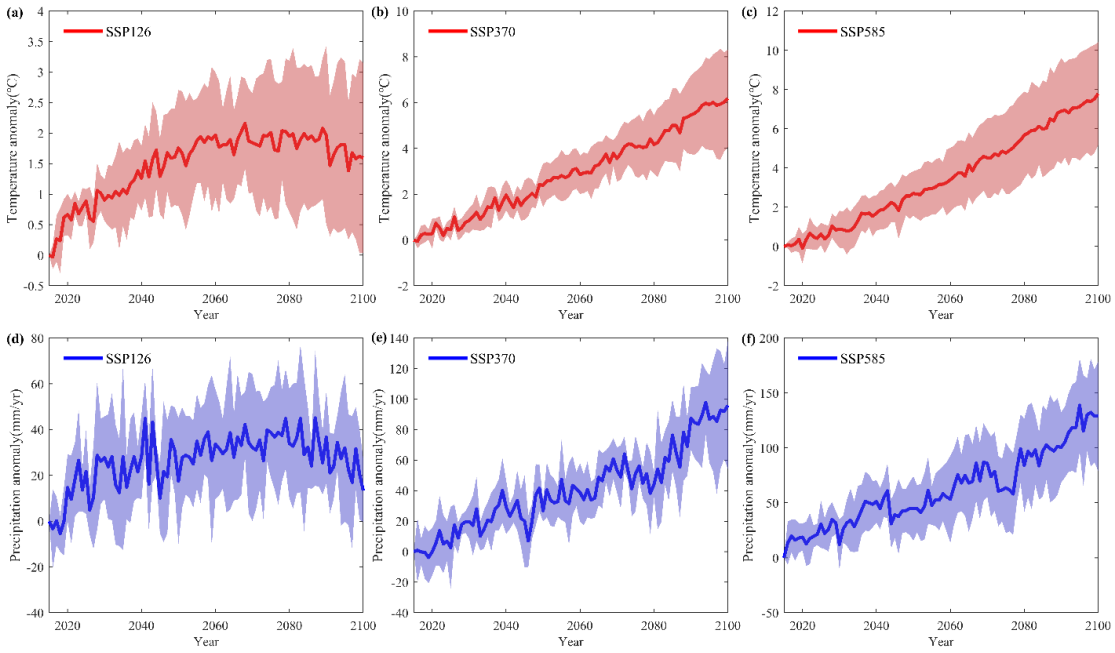

Fig. S19: Future variations in temperature and precipitation of the northern high latitudes under different SSP scenarios. Future temperature and precipitation data were from Inter-Sectoral Impact Model Intercomparison Project (ISIMIP) phase 3b, which were supplied based on Climate Model Intercomparison Project Phase 6 (CMIP6) output of five climate models: GFDL-ESM4, IPSL-CM6A-LR, MPI-ESM1-2-HR, MRI-ESM2-0 and UKESM1-0-LL.

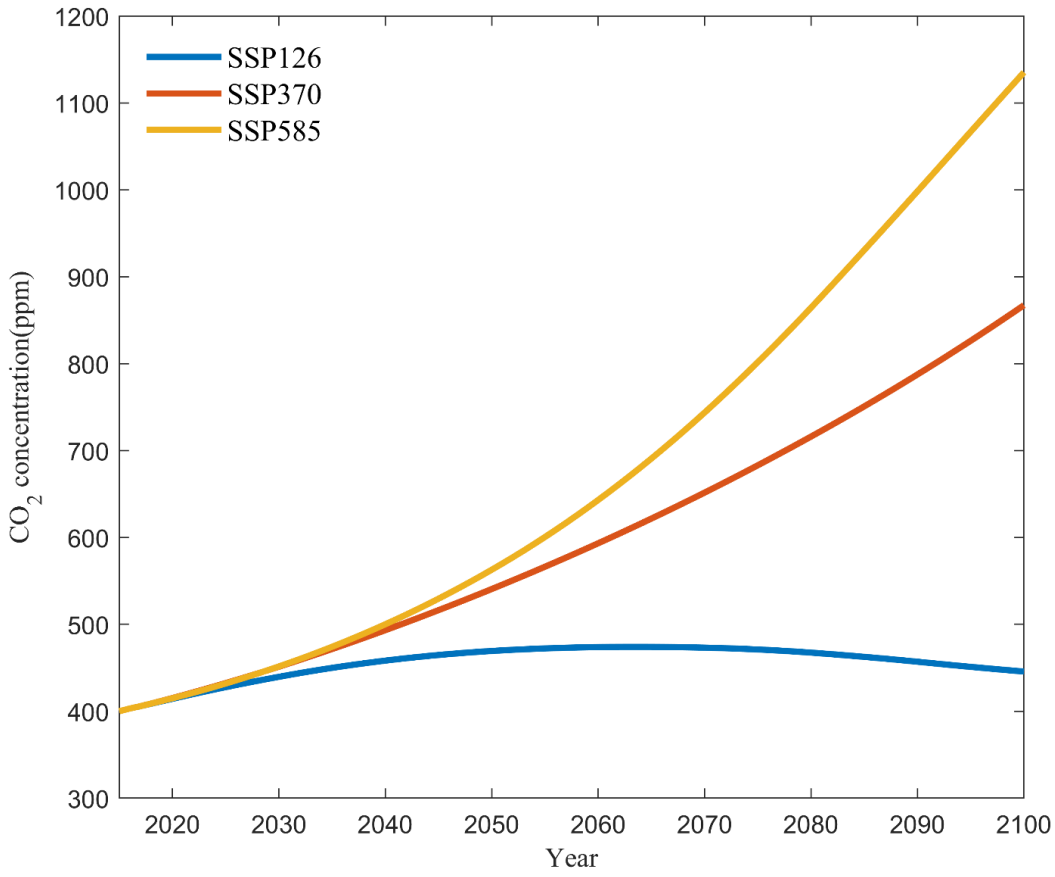

Fig. S20: Future variations in atmospheric CO_2 concentration under different SSP scenarios.

Table S1: Model simulation design

Historical	Climate	CO_2	LULCC	N deposition	N fertilizer	Manure N
S0	1901-1920	1860	1860	1860	1860	1860
S1	•	•	•	•	•	•
S2	•	•	•	•	•	1860
S3	•	•	•	•	1860	1860
S4	•	•	•	1860	1860	1860
S5	•	•	1860	1860	1860	1860
S6	•	1860	1860	1860	1860	1860

Note: "•" indicates the forcing during 1860-2016 is included in the simulation, "1901-1920" indicates the 20-year mean climate condition during 1901-1920 was used over the entire simulation period, and "1860" indicates the forcing was fixed in 1860 level over the entire period. Climate data was only available from 1901, we used the 20-yr average value between 1901 and 1920 for years 1860-1900.

Table S2: Spatial and temporal resolution of bottom-up and top-down models used in this study.

Bottom-up estimates				
Name	Sector	Spatial resolution	Temporal coverage	References
DLEM	Soil	0.5°×0.5°	1860-2016	Tian et al. (2015)
LPJ-GUESS	Soil	0.5°×0.5°	1860-2016	Olin et al. (2015)
LPX-Bern	Soil	0.5°×0.5°	1860-2016	Stocker et al. (2013)
O-CN	Soil	1°×1°	1860-2016	Zaehle et al. (2011)
ORCHIDEE-CNP	Soil	2°×2°	1860-2016	Goll et al. (2017)
VISIT	Soil	0.5°×0.5°	1860-2016	Inatomi et al. (2010)
EDGARv6.0	Multiple sources (see method)	0.1°×0.1°	1970-2018	Crippa et al. (2019)
GFED4.1s	Biomass burning	0.25°×0.25°	1997-2021	Van Der Werf et al. (2017)
Top-down estimates				
Name (ACTM)	Resolution of state vector	ACTM horizontal resolution	Temporal coverage	References
GEOSChem	5°×4°	5°×4°	1998-2016	Wells et al. (2018)
INVICAT	5.625°×5.625°	5.625°×5.625°	1998-2014	Wilson et al. (2014)
MIROC4-ACTM	84 regions	2.8°×2.8°	1998-2016	Patra et al. (2018)

References

Crippa, M., Oreggioni, G., Guizzardi, D., Muntean, M., Schaaf, E., Lo Vullo, E., Solazzo, E., Monforti-Ferrario, F., Olivier, J. G. J., & Vignati, E. (2019). Fossil CO2 and GHG emissions of all world countries. *Publication Office of the European Union: Luxemburg*.

Goll, D. S., Vuichard, N., Maignan, F., Jornet-Puig, A., Sardans, J., Violette, A., Peng, S., Sun, Y., Kvakic, M., Guimberteau, M., Guenet, B., Zaehle, S., Penuelas, J., Janssens, I., & Ciais, P. (2017). A representation of the phosphorus cycle for ORCHIDEE (revision 4520). *Geosci. Model Dev.*, *10*(10), 3745-3770. https://doi.org/10.5194/gmd-10-3745-2017

Inatomi, M., Ito, A., Ishijima, K., & Murayama, S. (2010). Greenhouse gas budget of a cool-temperate deciduous broad-leaved forest in Japan estimated using a process-based model. *Ecosystems*, *13*(3), 472-483.

Olin, S., Lindeskog, M., Pugh, T. A. M., Schurgers, G., Wårlind, D., Mishurov, M., Zaehle, S., Stocker, B. D., Smith, B., & Arneth, A. (2015). Soil carbon management in large-scale Earth system modelling: implications for crop yields and nitrogen leaching. *Earth System Dynamics*, *6*(2), 745-768.

Patra, P. K., Takigawa, M., Watanabe, S., Chandra, N., Ishijima, K., & Yamashita, Y. (2018). Improved chemical tracer simulation by MIROC4. 0-based atmospheric chemistry-transport model (MIROC4-ACTM). *Sola*, *14*, 91-96.

Stocker, B. D., Roth, R., Joos, F., Spahni, R., Steinacher, M., Zaehle, S., Bouwman, L., & Prentice, I. C. (2013). Multiple greenhouse-gas feedbacks from the land biosphere under future climate change scenarios. *Nature Climate Change*, *3*(7), 666-672.

Tian, H., Chen, G., Lu, C., Xu, X., Ren, W., Zhang, B., Banger, K., Tao, B., Pan, S., & Liu, M. (2015). Global methane and nitrous oxide emissions from terrestrial ecosystems due to multiple environmental changes. *Ecosystem Health and Sustainability*, *1*(1), 1-20.

Van Der Werf, G. R., Randerson, J. T., Giglio, L., Van Leeuwen, T. T., Chen, Y., Rogers, B. M., Mu, M., Van Marle, M. J. E., Morton, D. C., & Collatz, G. J. (2017). Global fire emissions estimates during 1997-2016.

Wells, K. C., Millet, D. B., Bousserez, N., Henze, D. K., Griffis, T. J., Chaliyakunnel, S., Dlugokencky, E. J., Saikawa, E., Xiang, G., Prinn, R. G., O'Doherty, S., Young, D., Weiss, R. F., Dutton, G. S., Elkins, J. W., Krummel, P. B., Langenfelds, R., & Steele, L. P. (2018). Top-down constraints on global N2O emissions at optimal resolution: application of a new dimension reduction technique. *Atmos. Chem. Phys.*, *18*(2), 735-756. https://doi.org/10.5194/acp-18-735-2018

Wilson, C., Chipperfield, M. P., Gloor, M., & Chevallier, F. (2014). Development of a variational flux inversion system (INVICAT v1. 0) using the TOMCAT chemical transport model. *Geoscientific Model Development*, *7*, 2485-2500.

Zaehle, S., Ciais, P., Friend, A. D., & Prieur, V. (2011). Carbon benefits of anthropogenic reactive nitrogen offset by nitrous oxide emissions. *Nature Geoscience*, *4*(9), 601-605.